

SIMULATION AND ANALYSIS OF MICROBUNCHING INSTABILITY IN A HIGH REPETITION RATE FEL BEAM DELIVERY SYSTEM*

J. Qiang[†], J. Corlett, P. Emma, C. E. Mitchell, and M. Venturini, LBNL, Berkeley, CA 94720, USA

Abstract

The microbunching instability in the accelerator beam delivery system of an FEL can significantly degrade the electron beam quality and limit the performance of the X-ray radiation. In this paper, we present detailed numerical simulation and analysis of the microbunching instability in a high repetition rate X-ray FEL beam delivery system that is being studied at Lawrence Berkeley National Laboratory. Our results suggest that by using a flexible accelerator design and a laser heater, the effects of the microbunching instability can be suppressed without significantly sacrificing the final electron beam quality.

INTRODUCTION

A high repetition rate, soft X-ray free electron laser, Next Generation Light Source is being studied at LBNL to generate radiation in an array of FEL beam lines [1]. The FEL driver consists of a 2.4 GeV superconducting 1.3GHz Linac and a low RF frequency (187 MHz) high repetition rate (1 MHz or higher) normal conducting gun. The 300pC bunches are compressed to a 500-600A peak current by velocity bunching in the injector and magnetic chicanes at 215 and 720 MeV beam energy (compression factors of 10, 2, and 5 respectively [2]).

The microbunching instability is of concern particularly with regard to the performance of the externally seeded FEL beamlines, which critically depends on small beam slice energy spread and avoidance of nonlinear energy chirp. We used high-resolution multi-billion macroparticle start-to-end simulations enabled by the Impact code [3] to study the microbunching instability seeded by shot noise as well as small current perturbations at the cathode (caused, for example, by non-uniformities in the photo-gun laser pulse).

MICROBUNCHING IN THE INJECTOR

We modeled the effect of irregularities in the photo-gun laser profile by placing few-percent sinusoidal modulations of given period on the nominal beam current generated at the cathode. We studied in detail the evolution of these modulation by monitoring the amplitude of the excited mode along the injector, see Fig. 1 for two choices of perturbation period, as indicated. The simulations show some magnification in the amplitude of the modulation, while the beam undergoes compression by velocity bunching.

* Work supported by the U.S. Department of Energy under Contract No. DE-AC02-05CH11231 using computing resources at the NERSC.

[†] jqiang@lbl.gov

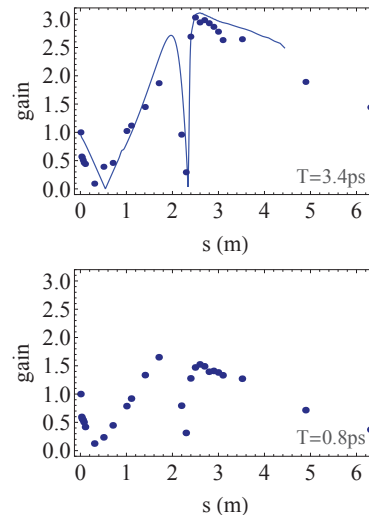


Figure 1: Initial sinusoidal perturbation gain evolution inside the injector from the IMPACT simulations (dots) and the linear model (line).

We attempted to model the evolution of these modulations with a simple, linear 1D model aiming at capturing the qualitative behavior of the longitudinal beam dynamics through the first few meters of the injector, including the buncher, the downstream drift, and the first cavity of the booster. We describe the particle dynamics in terms of $(\Delta z, \Delta p_z)$, deviations from the reference orbit, where Δz is the longitudinal coordinate and $\Delta \tilde{p}_z = \Delta p_z / mc$ is the scaled longitudinal momentum. Time is the independent variable. We denote M as the 2×2 matrix for the linear unperturbed motion (no space-charge). Through a drift space (including the gun gap, where all beam particles experience about the same accelerating field) the non-trivial entry of the matrix reads $M_{12}(t' \rightarrow t) = c \int_{t'}^t dt' / \gamma^3(t')$. We model the buncher as a thin cavity operated at zero-field crossing, with transfer matrix $M_{11} = M_{22} = 1$, $M_{12} = 0$ and $M_{21} = -\alpha_B$, and assume that the beam stays on crest through the first cavity of the buncher (implying that all the RF compression is induced by the buncher, which is close to a typical set-up for the NGLS injector). The compression factor at time t is $C(t) = 1$ for $t < t_B$ and $C(t) = |1 - \alpha_B M_{56}(t_B \rightarrow t)|^{-1}$ for $t > t_B$, where t_B is the time the reference particle reaches the buncher. The parameter α_B , is adjusted empirically so as to yield a compression factor profile along the injector that is comparable to that resulting from the IMPACT simulations (see Fig. 2).

The bunching function relative to the nominal wavenum-

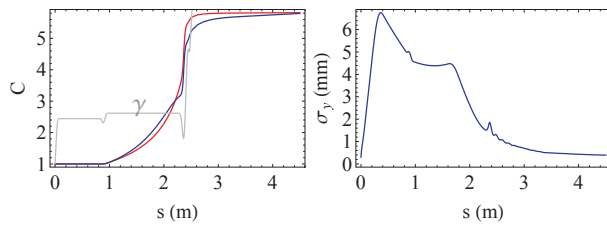


Figure 2: Left: compression factor from model (red) and IMPACT simulations (blue). Right: transverse rms beam size.

ber k_0 is found as the solution of the integral equation

$$b = b_0 + \int_0^t dt' K(t', t) b(t') \quad (1)$$

where $k = C(t)k_0/\beta(t)$ and $k' = C(t')k_0/\beta(t')$, and the kernel reads

$$K = 4\pi i \frac{C(t')I(t')}{I_A} M_{12}(t' \rightarrow t) \beta(t') k \frac{Z(k', s)}{Z_0} \quad (2)$$

Space charge is described by the 1D model $Z(k) = Z_0[1 - 2K_1(x)I_1(x)]/k\pi r_b^2$ where $x = kr_b/\gamma$ and r_b is an effective transverse beam radius. The evolution of the relative amplitude of the sinusoidal charge density perturbation from the model is shown in Fig. 1 as the solid line. For the case of longer perturbation period (top picture) the model roughly overlaps with the simulation data (dots) provided that we choose $r_b(t) = 2.1\sigma_\perp(t)$, where $\sigma_\perp(t)$ is the rms transverse beam size as determined by the IMPACT simulations. The mode amplitude is in units of the amplitude observed in the beam core at the time the beam tail leaves the cathode. The behavior of the mode as observed in the figure has the signature of a plasma oscillation with increasing period as the beam undergoes acceleration. The evolution of the perturbation with shorter ($T=0.8$ ps) period, bottom picture, exhibits a similar plasma oscillation period (consistent with the 1 D model) but a reduced gain.

MICROBUNCHING INSTABILITY THROUGH THE LINAC

The microbunching instability gain at the exit of the second bunch compressor is calculated as a function of the initial modulation wavelength following a linear theory and is shown in Fig. 3 for three different initial uncorrelated energy spreads. It is seen that with an initial 5 keV uncorrelated energy spread, the peak of the gain can be higher than 1000 with an initial modulation wavelength of about 40 μm . An increase of the initial uncorrelated energy spread to 15 keV significantly reduces the gain of the instability to below 100. Figure 4 shows the final electron beam longitudinal phase space distribution from a direct start-to-end numerical simulation using the real number of electrons (laser heater was not included in the simulation). The microbunching instability starting from the electron beam

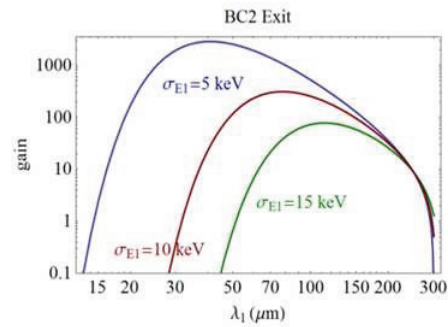


Figure 3: Gain of the microbunching instability at the exit of the second bunch compressor through the linac as a function of the initial modulation wavelength.

shot noise causes large phase space filamentation and increased energy spread of the final electron beam. This will result in the degradation of the FEL performance with less radiation power and larger radiation bandwidth.

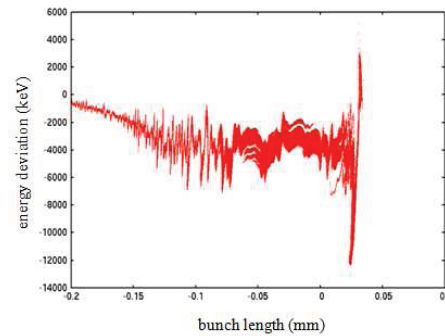


Figure 4: Final electron beam longitudinal phase space distribution from a direct start-to-end numerical simulation without the laser heater.

As suggested from the gain curve of the linear theory in Fig. 3, the microbunching instability can be significantly suppressed by a larger initial uncorrelated energy spread, which can be attained with the use of a laser heater [4]. Figure 5 shows the final electron beam current profiles at

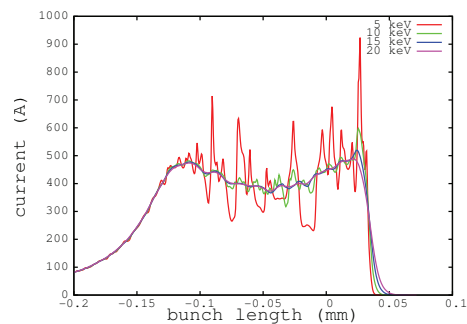


Figure 5: Final electron beam current profiles with different initial uncorrelated energy spread.

the entrance of undulator radiators with different values of

the initial uncorrelated energy spread from the laser heater. It appears that 15 keV uncorrelated energy spread is needed in order to suppress the microbunching instability. Figure 6

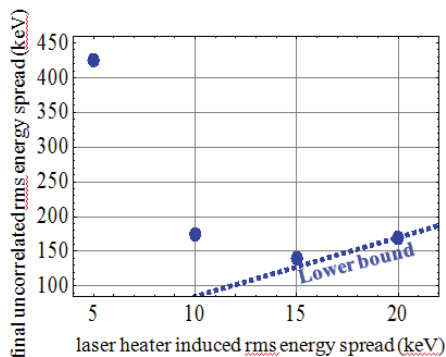


Figure 6: Final electron beam uncorrelated energy spread as a function of the initial energy spread from the laser heater.

shows the final electron beam uncorrelated energy spread as a function of the initial energy spread from the laser heater. The use of the 15 keV initial energy spread leads to a minimum about 150 keV final uncorrelated energy spread.

Besides using the laser heater, an alternative way to mitigate the microbunching instability is to use a single bunch compressor (BC1) in the accelerator beam delivery system. Figure 7 shows the final electron beam longitudinal phase space distribution with the single bunch compressor from direct numerical simulation. It is seen that the microbunching instability is much weaker than that in the two bunch compressor case. Only 10 keV initial uncorrelated energy spread is needed to suppress the microbunching instability through the linac.

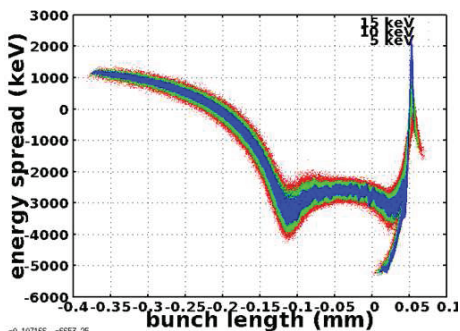


Figure 7: Final electron beam longitudinal phase space distribution with different initial energy spread through the linac with a single bunch compressor.

In addition to the current modulation starting from the electron beam shot noise, the initial laser temporal profile rippling also results in current modulation. Figure 8 shows final electron beam current profiles with an initial 5% temporal laser modulation and different modulation periods

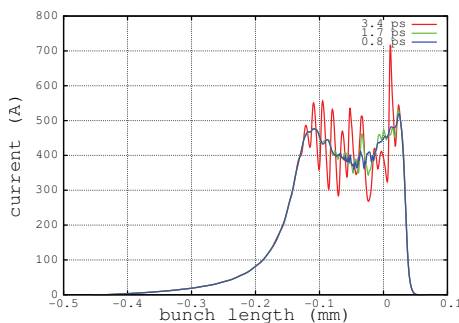


Figure 8: Final electron beam current profiles with initial 5% temporal laser modulation and different modulation periods through the nominal two bunch compressor linac.

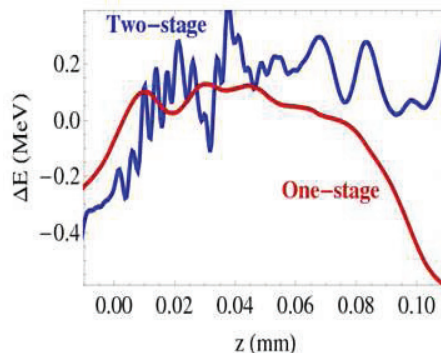


Figure 9: Final beam slice (average) energy with one and two bunch compressor. Microbunching instability seeded by 5% amplitude beam density modulation at cathode.

through the nominal two bunch compressor linac with initial 15 keV energy spread from the laser heater. The longer temporal period (3.4 ps) causes significant microbunching instability while the initial shorter period modulation is significantly damped.

The microbunching instability not only causes final electron beam current modulation but also slice energy modulation that results in an increase of the X-ray FEL radiation bandwidth. Figure 9 shows the final electron beam slice energy at the exit of the spreader through the single and the double bunch compressor linac with an initial 5%, 0.8 ps laser temporal modulation. The microbunching instability in the single bunch compressor linac is much weaker and the resulting final slice energy is also much smoother.

REFERENCES

- [1] J. Corlett, et al., “Next generation light source R&D and design studies at LBNL,” in Proceedings of IPAC 2012.
- [2] M. Venturini, et al., “Beam Dynamics Studies of a High-repetition Rate Linac Driver for a 4th-generation Light Source,” in Proceedings of IPAC 2012.
- [3] J. Qiang et al., J. Comp. Phys. vol. 163, 434, (2000); J. Qiang et al., Phys. Rev. ST Accel. Beams 12, 100702 (2009).
- [4] Z. Huang et al., Phys. Rev. ST Accel. Beams 13, 020703 (2010).